Effects of Flow on Morphological Stability During Directional Solidification

S.H. DAVIS and T.P. SCHULZE

Research involving the interaction of flow with morphological instability during directional solidification of binary alloys is reviewed. In general, flow may arise during the solidification process from thermal and solutal buoyancy, changes in density upon solidification, thermocapillary forces at free boundaries, or external forcing of the system. We focus primarily on the last of these, giving details of the influence of various forced flows on the critical conditions for morphological instability. These flows include the asymptotic suction profile, stagnation-point flow, and periodically driven shear flows. Parallel shear flows are unable to stabilize morphological instabilities in three dimensions but may lead to new long-wave, traveling instabilities. Flow-induced, long-wave instabilities are also encountered in the presence of both steady and modulated stagnation-point flows. Unsteady, nonparallel shear flows may stabilize morphological instability if the flow parameters are adjusted properly.

I. INTRODUCTION

SOLID to liquid phase transformation involves a complex interplay of many physical effects. The solid/liquid interface is an active boundary from which latent heat is liberated during phase transformation. This heat is conducted away from the interface through the solid and liquid, establishing thermal boundary layers near the interface. If the liquid is not pure but contains solute, then preferential rejection or incorporation of solute occurs at the interface. For example, if there is a single solute present and its solubility is smaller in the (crystalline) solid than it is in the liquid, the solute will be rejected at the interface. This rejected material is diffused away from the interface through the solid and liquid setting up concentration boundary layers near the interface. The thermal and concentration boundary layer distributions determine, in part, whether there exist morphological instabilities of the interface.

Fluid flow may also have a strong influence on interface morphology. In general, there are four different sources of flow within the melt. If the solidification process is occurring in a gravitational field, the thermal and solutal gradients induce buoyancy-driven convection that is known to greatly affect the interfacial patterns and hence the solidification microstructures that are present in the solidified material.[1] If the solidification process involves fluid-fluid interfaces, such as those found in containerless processing in a microgravity environment, then variations in surface tension along these interfaces may drive convection in the melt. Flow normal to the solidifying interface will be created by the expansion or contraction of material upon solidification. Finally, the presence of external forces may stir the melt. Brown[2] gives a broad survey of the processing configurations and the types of flows that occur.

There are several categories of problems that have received quantitative study. The first area, which we call *prototype flows*, involves simple flow geometries that correspond to well-studied hydrodynamic instabilities. If one (or more) of the rigid boundaries of such a geometry is replaced by a crystal interface, and if temperature and / or concentration gradients are posed to support this, then one can investigate the influence of heat and mass transfer on the morphology of the interface(s). Here, it is usually supposed that the liquids are "pure" and the interfaces in their basic states are supposed stationary. Thus, even though morphological changes are important and these studies involve morphological instabilities, these should not be confused with *the* morphological instability of moving fronts which may occur even in the absence of flow. Prototype flows have been amply reviewed in Glicksman *et al.*[3] and Davis.[4,5]

The second area involves the morphological instability in binary alloys during *directional solidification.* Here, the primary instability is driven by solute rejection and the resulting solute distribution near the propagating interface. Thermo-soluto convection driven by gravity can couple strongly with the interface. These interactions have been reviewed in Davis.[4,5]

The third area involves the study of imposed flows during directional solidification. These flows have the potential of homogenizing the solute distribution and hence delaying the onset of morphological change. However, the interaction of flows with interfaces can also generate new instabilities that promote morphological changes. Such flows are the principle subject of this review.

There are several surveys that would be useful to consult: Carruthers,[6,7,8] Hurle,[9] Solan and Ostrach,[10] Pimputkar and Ostrach,[11] Kobayashi,[12] Azouni,[13] Rosenberger,[14] Ostrach,[15] Langlois,[16,17] Coriell *et al.*,[18] Glicksman *et al.*,[3] and Davis.[4,5]

II. DIRECTIONAL SOLIDIFICATION OF BINARY LIQUIDS

Directional solidification is concerned with a front moving at constant speed. A typical experimental configuration has two constant-temperature sources which are fixed in a laboratory frame. A binary liquid fills the region between

S.H. DAVIS, Walter P. Murphy Professor of Applied Mathematics, is with the Department of Engineering Sciences and Applied Mathematics, Northwestern University, Evanston, IL 60208. T.P. SCHULZE, Postdoctoral Fellow, is with the Department of Applied Mathematics and Theoretical Physics, University of Cambridge, Cambridge, England CB3 9EW.

This article is based on a presentation made at the "Analysis and Modeling of Solidification" symposium as part of the 1994 Fall meeting of TMS in Rosemont, Illinois, October 2–6, 1994, under the auspices of the TMS Solidification Committee.

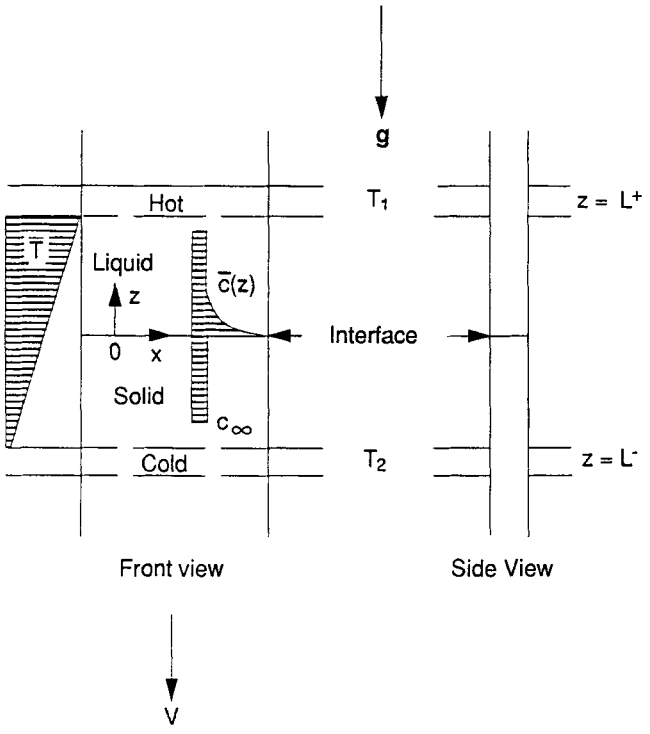

Fig. 1—Directional solidification without flow: Configuration for directional solidification in a Hele–Shaw cell. The mean position of the interface is $z = 0$, and the temperature T is linear in the frozen-temperature approximation; $T_1 > T_2$.

closely spaced parallel plates forming a Hele–Shaw cell. When the plates are laid across the heat sources, the material solidifies at a position where the local temperature equals the melting (or solidification) temperature T_m; the interface is planar in this static configuration. The plates are now pulled through the temperature gradient, at constant speed V, so that the liquid is continuously solidified. After transients have disappeared, the solid/liquid interface remains stationary in the laboratory frame, since it is "pinned" at $T = T_I$, which now differs somewhat from the T_m in the static state since it depends on the local concentration (constitutional undercooling) and the velocity of the interface (kinetic undercooling). This configuration is widely used for detailed experiments with organic binary liquids, since the material is transparent and the thin-domain geometry allows *in situ*, optical viewing of the interface. To be sure, the growth of single crystals commercially or in natural contexts involves the growth in fully three-dimensional geometries of opaque metallic or semiconductor materials.

It is known on the bases of theory[19] and of experiment[20,21,22] that the interface remains planar during solidification of binary liquids at nonzero values of the pulling speed V until a first critical value V_c is attained. Near V_c, nearly two-dimensional steady cells will appear, and these deepen as V is increased. As V is increased further, there is a dendritic transition in which deep cells develop side-branches. Finally, there is a second critical value of V, $V = V_A$, the absolute stability limit; as $V \to V_A$, these dendritic structures fade to cells, and the cells fade further until the planar interface regains stability. Langer[23] gives an overview of these events and also discusses solidification phenomena that occur in other contexts.

The pure morphological instability in unidirectional solidification is diffusive in nature, being driven by the adverse gradient of solute concentration C at the interface. The onset of cellular structure creates lateral variations in C in the liquid, and when solute is rejected, the concentration is elevated in the troughs of the cells. When the grooves between cells are deep, the solute is trapped there; the large path lengths from the root to the bulk liquid above make longitudinal diffusion very slow compared to the rate of growth at the tip. The solidified material will inherit these nonuniformities, a set of high-concentration stripes parallel to the growth direction. The stripes extend downward until a new phase is encountered.

When the liquid is flowing, the solute distribution is altered. It may be homogenized and so delay the morphological instability. If the flow is unsteady, say, time periodic, both temperature and concentration oscillations will be present. These oscillations cause the modulation of the boundary-layer thicknesses and of the growth speed V. These, in turn, will create variations in concentration in the solid, resulting in bands of material varying in concentration which are referred to as "striations," perpendicular to the growth direction. Oscillatory motion in the liquid is one of the most frequent causes of crystalline inhomogeneities.[1]

In the present article, we investigate the effects of hydrodynamics in directional solidification. We find that the flow can alter the critical conditions for the onset of morphological instability. It can create scale and pattern changes in the morphology. It can create, through coupling, new instabilities that pre-empt the old and give new criteria for morphological changes. In Section III, we outline the pure morphological-instability problem. In Section IV, we examine forced flows imposed on interfaces and highlight flow-induced morphological instabilities. Section V gives a closing discussion.

III. MORPHOLOGICAL INSTABILITIES

Figure 1 shows a directional-solidification cell in which a binary liquid undergoes phase transformation at melting temperature T_I. Fluid motion is absent and, for simplicity of presentation, the system is taken to be two-dimensional. We consider the case of solute rejection so that the distribution coefficient k satisfies $0 \le k < 1$. We further invoke[23] the "frozen-temperature approximation" which gives the temperature T in the solid and liquid permanently by

$$T = T_0 + Gz \qquad [1]$$

where G is the (imposed) temperature gradient, z is the coordinate along the temperature gradient, and T_0 is a reference temperature.

Eq. [1] is a good approximation when (1) the latent heat liberated at the interface is conducted away much faster than the interface advances (small Stefan number), (2) the solute diffusion is much slower than the thermal conduction (so that on small length scales solute effects are rate limiting), and (3) the thermal conductivities are taken to be equal. The details of the thermal field are usually, but not always, unimportant in directional solidification. For example, in rapid solidification, the frozen-temperature approximation is often a poor one.

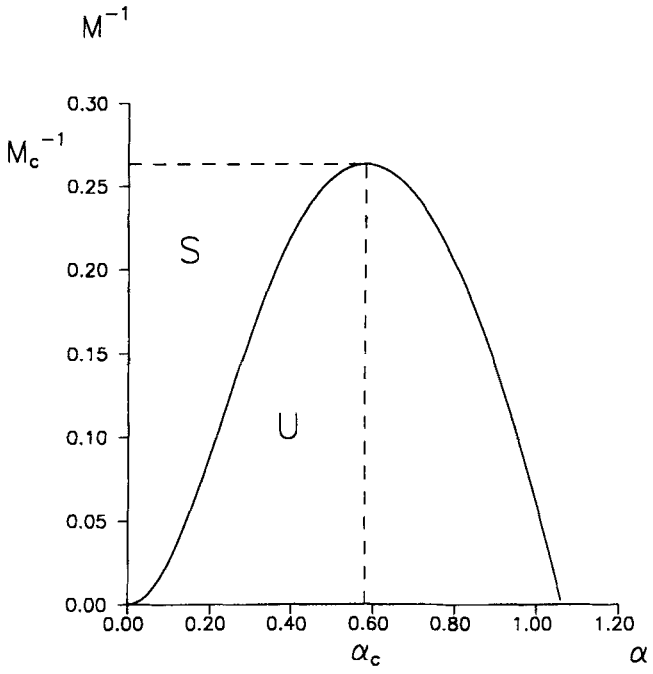

Fig. 2—Directional solidification without flow: M^{-1} *vs* α for $S = 81.0$, $k = 0.3$, and $\Gamma = 0.6$. The region above the curve corresponds to a stable (S) interface, and the region below the curve corresponds to an unstable (U) interface.

Given that the temperature field is passive, it is only the solute concentration C in the liquid that can be perturbed. We consider the problem in the frame of reference moving with the planar interface. The instability is driven at the interface $z = h(x,t)$, where jump conditions are obtained using the assumption of local thermodynamic equilibrium. The temperature T_I on the interface is given by the Gibbs–Thomson equation. The other boundary conditions are a balance of solute across the interface and an appropriate far-field condition.

There is a steady basic state that consists of a planar interface $\bar{h} = 0$, a constant concentration in the solid $C_S = C_\infty$, and a concentration boundary layer in the liquid

$$\overline{C} = C_\infty \left[1 + \frac{1 - k}{k} e^{-\frac{z}{\delta_c}}\right] \qquad [2]$$

where $\delta_C = D/V$, the ratio of the solute diffusivity to the pulling speed.

In actuality, the basic state has exponential structure in both C and T, with the concentration and thermal boundary layers having thicknesses δ_C and $\delta_T = \kappa_L/V$, respectively. Here, κ_L is the thermal diffusivity in the liquid. However, usually $\kappa_L >> D$ and the thermal profile near the interface becomes linear.

The instability of the planar basic state was explained first by Tiller *et al.*,[24] and a full linear-stability theory, including the effects of surface energy, was first given by Mullins and Sekerka.[19] Coriell and McFadden[28] give a survey of past results.

The mechanism can be explained[19] by examining an initially corrugated interface in a background basic state $\overline{C}$. A bump of solid pushes its front into a higher temperature environment and thus tends to melt back; the temperature distribution is stabilizing. A bump of solid is concave toward the solid and so, by the Gibbs–Thomson effect, has its local melting point decreased; surface energy is stabilizing. A bump of solid will protrude into a region of reduced solute concentration due to the effect of solute rejection. Thus, the local melting temperature near a bump will be reduced due to constitutional undercooling and continued growth will be favored. This last effect can be related to the (negative) concentration gradient at the interface G_C, with larger values of $|G_C|$ indicating a greater tendency for interfacial instability.

It is know that G_C is given by

$$G_C = -\frac{1 - k}{k} \frac{C_\infty V}{D} \qquad [3]$$

We see that $|G_C|$ increases with increasing pulling rate V and with increased concentrations C_∞ of solute present. It decreases the faster the diffusion removes the rejected solute from the interfacial region. When $k \to 0$, all of the solute is rejected from the solid and $|G_C|$ is large. When $k \to 1$, and hence $G_C \to 0$, there is no rejection, $C_S = C_L$, and hence no morphological instability.

The stability index can be expressed as the ratio M:

$$M = \frac{mG_C}{G} \qquad [4]$$

which we refer to as the morphological number. Here, G is the thermal gradient and m is the liquidus slope in the phase diagram. The morphological number is then essentially a ratio of the destabilizing concentration gradient to the stabilizing thermal gradient. The liquid is constitutionally undercooled if $M > 1$. When surface energy is present, the condition for instability[19] is $M > M_c$, where $M_c > 1$ and the value of M_c depends on a surface energy parameter Γ and the segregation coefficient k. Here,

$$\Gamma = \frac{T_M \gamma V^2}{L_V m G D^2} \qquad [5]$$

where γ is the surface energy per unit area on the interface.

In Figure 2, we present a typical neutral curve, plotting M^{-1} as a function of the disturbance wavenumber α for parameter values characteristic of a lead-tin alloy. For a given wavenumber α, if M^{-1} is above (below) this curve, disturbances with that wavenumber will decay (grow). For the system to be linearly stable, M^{-1} must be above this curve for all wavenumbers. As one decreases M^{-1}, the instability will set in at the critical wavelength, α_c.

With k fixed, the neutral curve depends only on the surface-energy parameter Γ. In Figure 2, we use the value $\Gamma = 0.6$. In Figure 3, we plot the critical value of M^{-1} as a function of Γ. The nondimensional critical wavenumber approaches infinity as $\Gamma \to 0$ along these curves and approaches zero as Γ is increased. The system is absolutely stable for $\Gamma > 1/k$, referred to as the absolute stability limit, Γ_s.

In Figure 4, we reproduce the information in the M^{-1} *vs* Γ plot from Figure 3 but in terms of the dimensional quantities V, the pulling speed, and C_∞, the far-field concentration, for fixed temperature gradient, G. When experiments are performed, the pulling speed is the most readily controlled parameter. As seen from this diagram, the interface will always be stable for sufficiently low concentrations of

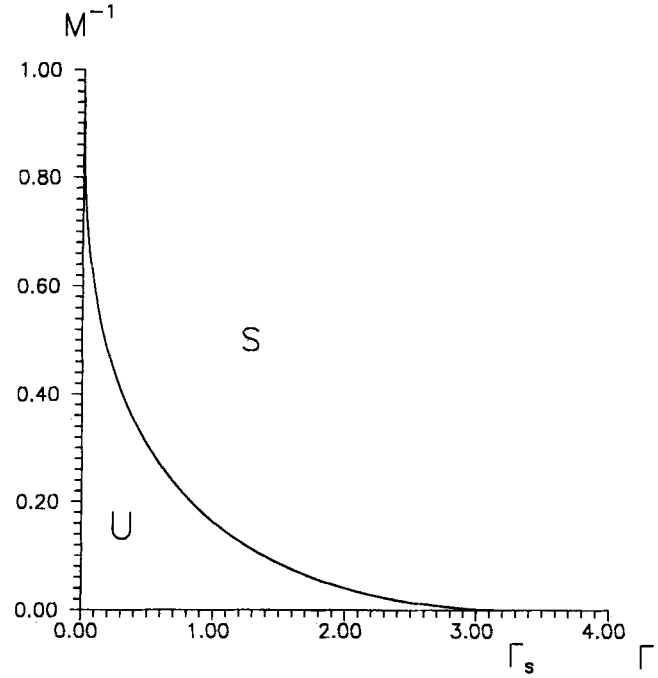

Fig. 3—Directional solidification without flow: The critical value (maximized over wavenumbers) of M_c^{-1} and the critical wavenumber as a function of Γ for $S = 81.0$ and $k = 0.3$. Stable (S) and unstable (U) regions lie above and below the M_c^{-1}-*vs*-Γ curve, respectively. The absolute stability limit is $\Gamma_s = 1/k$.

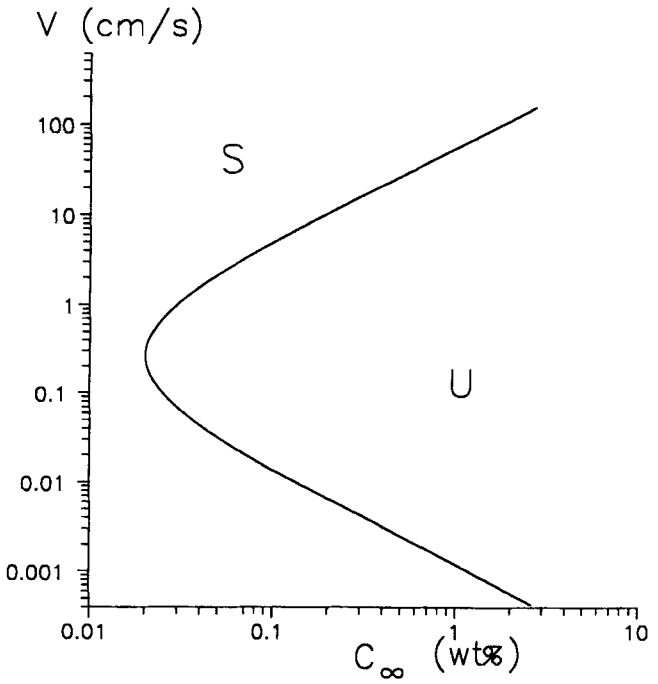

Fig. 4—Directional solidification without flow: V *vs* C_∞ with $k = 0.3$ and $G = 200$ K/cm. Stable (S) and unstable (U) regions lie to the left and right of the curve, respectively.

solute, but when the concentration is above some critical value, instability can set in for a range of pulling speeds.

There have been numerous studies of nonlinear cellular behavior: Wollkind and Segel,[25] Caroli *et al.*[26] and Alexander *et al.*[27] For a review of these and other articles on solidification without flow, see Coriell and McFadden.[28]

IV. FORCED FLOWS

The study of forced flows over solidifying interfaces aims at understanding how the solute redistribution by the flow alters morphological instabilities or creates new instabilities. Further, forced flows serve as a surrogate, allowing one to isolate certain effects of convection in the melt and focusing on one-way couplings.

There are many examples of forced flows. The crystal may be rotated to erase nonaxially symmetric thermal effects, but it creates a von Karman swirl flow. The use of microgravity environments for the growth of crystals suppresses major buoyancy effects, but vibrations of the spacecraft creates transient accelerations, called g-jitter, that stir the liquid. All of the previously mentioned flows are in a sense accidental or at any rate unintentional. They cannot be prevented or else are present, as in the case of the swirl, because the rotation is necessary for other reasons. There can also be intentionally imposed flows. In the mid-1960s, Hurle suggested that rather than crystal growers bemoaning the presence of convection as a source of crystal nonuniformities, they should try to "design" natural convection (or forced flows) that will homogenize the solute boundary layer at the interface. In effect, this would decrease the local gradient $|G_C|$ enough to eliminate the possibility of morphological instabilities. This attractive possibility has motivated a good deal of work on the coupling of flow and morphology.

A. *Steady Parallel Flows*

The first studies of forced flows were those of Delves,[29,30] who imposed a Blasius boundary layer on the interface; but by examining wave lengths short compared to the development length of the boundary layer, he really focused on locally parallel flow. Arguments of local parallelism led Coriell *et al.*[31] to impose plane Couette flow upon the interface.

If one pictures an imposed flow at "infinity" across an interface and allows the solidification to proceed, the interface acts as a porous boundary and the forced flow has what is known as the asymptotic-suction profile, a boundary-layer flow on the scale δ_ν, the viscous boundary-layer thickness:

$$\delta_\nu = \nu/V \qquad [6]$$

The velocity component along the interface has the form

$$u \propto 1 - e^{-z/\delta\nu} \qquad [7]$$

The linear-stability theory was examined by Forth and Wheeler.[32]

Given that the concentration and thermal boundary layers scale on δ_C and δ_T, there are three lengths involved in such problems. When one has an organic mixture, then

$$\delta_C << \delta_T << \delta_\nu \qquad [8]$$

since $\delta_\nu/\delta_T = \mathrm{Pr}$, and the Prandtl number Pr is large. However, if one has a small Prandtl number metallic alloy, then

$$\delta_C << \delta_\nu << \delta_T \qquad [9]$$

These inequalities are relevant when one considers disturbances of various wave lengths λ. The "normal" situation

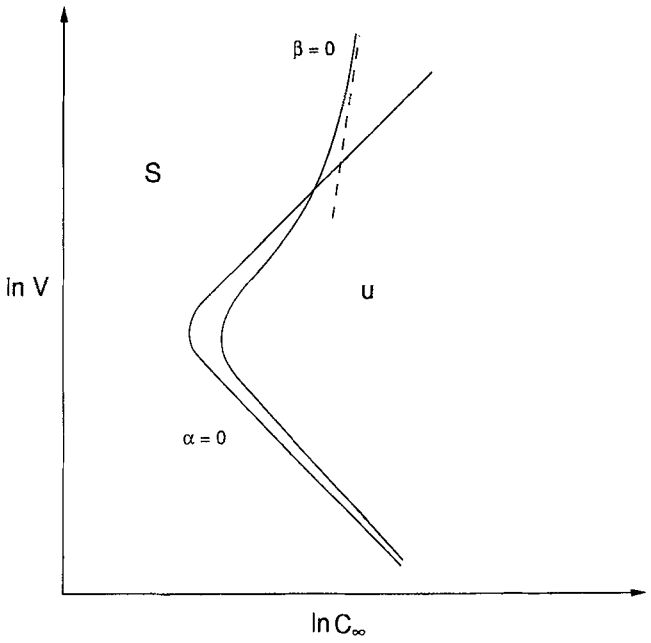

Fig. 5—Directional solidification into steady shear flow: Sketch of V *vs* C_∞ for fixed G for imposed parallel shear flow according to Hobbs and Metzener.[34] α and β are the wavenumbers in the flow and cross-flow directions. When the flow has a destabilizing effect, the cells will be periodic in the flow direction.

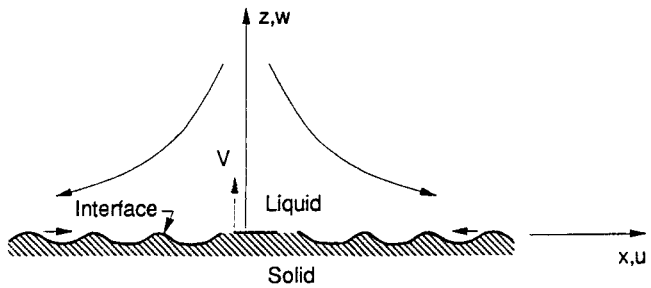

Fig. 6—Directional solidification into stagnation-point flow: Two-dimensional stagnation-point (Hiemenz) flow impressed upon a solidifying interface. The waves on the interface propagate toward the stagnation point according to Brattkus and Davis.[40]

described in Section II has $\lambda < \delta_C$ so that the thermal field and the velocity field can be represented in locally linear form

$$T = T_0 + Gz \qquad [10a]$$

$$u \sim Vz/\nu \qquad [10b]$$

the latter being the plane Couette flow considered by Coriell *et al.*[31] However, when λ becomes large enough, these localizations are no longer valid since the disturbances are affected by the curvatures of the profiles. Note that the distance L^+ from the interface to the upper heat source is a relevant length scale as well.

Coriell *et al.*[31] and Forth and Wheeler[32] examined two-dimensional disturbances (periodic in the flow direction) and found that the flow stabilizes the interface in that the presence of the flow increases M_c. However, if one considers longitudinal-roll disturbances (periodic cross stream and independent of the flow direction), the flow decouples from the problem and M_c is unchanged. Thus, under normal circumstances, the flow leaves M_c unchanged but selects the cellular state (longitudinal rolls) that appears.

Forth and Wheeler[33] have examined the weakly nonlinear development of two-dimensional waves and found that the flow promotes supercritical bifurcation and narrows the bandwidth of two-dimensional structures allowable in the nonlinear regime. Forth and Wheeler[32] have looked at a wider range of conditions and found for long waves that the flow destabilizes the interface for two-dimensional disturbances that propagate against the flow. However, they did not determine when this mode is preferred.

Hobbs and Metzener[34] have examined the effect of the asymptotic suction profile on the interface near the absolute stability boundary $V \approx V_A$. Here, the wave lengths are long compared to δ_C. Two-dimensional waves lower M_c and hence are preferred. Using the linear-stability theory, they establish conditions that determine neutral stability of the interface. Figure 5 shows that the neutral curve is somewhat stabilized along its lower branch and linear the nose but is substantially destabilized along the upper branch. Hobbs and Metzener[35] have extended their work into the nonlinear regime by examining parallel flow over an interface moving at $V \approx V_A$. Here, the long-wave structure of the solution induces a flow correction to the equation of Brattkus and Davis.[36] The resulting interface equation contains an extra linear term that accounts for the destabilization, but otherwise, the equation is left unchanged. When they specialize their equation to the weakly nonlinear regime, they obtain a modified Newell–Whitehead–Segel equation.[37,38] Further, when this equation is examined for phase evolution, a modified Kuramoto–Sivashinsky equation[39] is obtained, showing the presence of various sequences of normal, as well as chaotic, solutions.

B. *Nonparallel Flows*

Most flows, whether they occur naturally or as a result of stirring, are not parallel. These may include, for example, flow generated by rotation of the crystal or locally hyperbolic flows present when cellular convection exists at the interface.

Brattkus and Davis[40,41] studied two flows with hyperbolic streamlines directed upon a solidifying interface. These were, respectively, a von Karman swirl flow and stagnation-point flow. We discuss here the simplest of these, two-dimensional stagnation-point flow. Figure 6 shows the Hiemenz flow which, as $z \to \infty$, has the form

$$u \sim (K\nu)^{1/2} xF'(z),\ w \sim -(K\nu)^{1/2} F(z) \qquad [11]$$

where F is a function that is obtained numerically and K measures the strength of the flow. The linear-stability problem is made tractable by assuming that the viscous-boundary-layer thickness δ_ν is much larger than the concentration-boundary-layer thickness δ_C and that the Schmidt number S is very large. Explicitly, it is assumed that

$$\delta_C/\delta_\nu \equiv \left(\frac{D}{V}\right)\left(\frac{\nu}{K}\right)^{-1/2} = O(S^{-1/3}) \qquad [12]$$

as $S \to \infty$. Note that δ_ν here is different from that defined earlier. Given the smallness of δ_C, the interface senses only the local forms of the imposed flow and the flow senses a

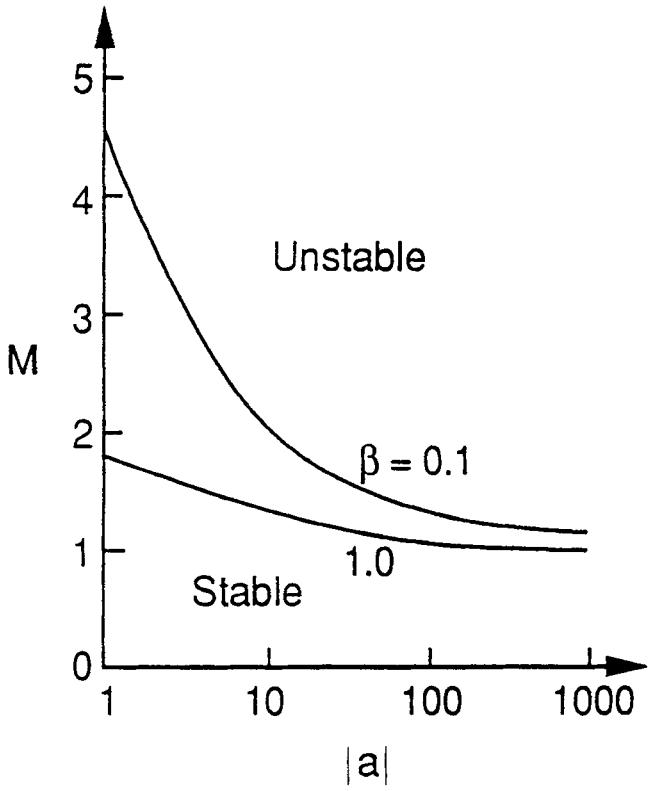

Fig. 7—Directional solidification into stagnation-point flow: Neutral curve, M *vs* $|a|$, for long two-dimensional disturbances on a Hiemenz flow against a solidifying interface according to Brattkus and Davis[40,41] for $k = 0.3$. Here, β is a nondimensional measure of the shear stress exerted by the Hiemenz flow on the interface.

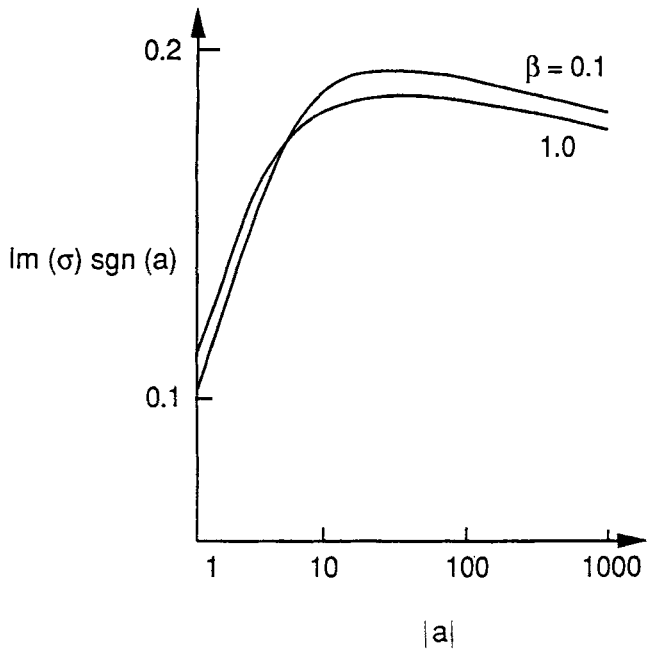

Fig. 8—Directional solidification into stagnation-point flow: Disturbance angular frequency *vs* $|a|$ on the neutral curve for long two-dimensional disturbances on a Hiemenz flow against a solidifying interface according to Brattkus and Davis[40,41] for $k = 0.3$. Here, β is a nondimensional measure of the shear stress exerted by the Hiemenz flow on the interface.

flat interface; thus,

$$u \sim \beta x \zeta \qquad [13a]$$

$$w \sim -\frac{1}{2}\beta\zeta^2 \qquad [13b]$$

where $\zeta = z/\delta_C$ and β measures $F''(0)$, the local shear. Finally, Brattkus and Davis considered waves long compared to δ_C though smaller than δ_v. They solved the modified diffusion problem

$$C_{\zeta\zeta} + (1 + \frac{1}{2}\beta\zeta^2)C_\zeta - \beta x \zeta C_x = C_\tau,\ 0 \le \zeta < \infty \qquad [14a]$$

$$C_\zeta + (1 - M^{-1})C_\tau + [k(1 - M^{-1})^{-1} + (1 - k)]C = 0 \quad \zeta = 0 \qquad [14b]$$

$$C = 0,\ \zeta \to \infty \qquad [14c]$$

where τ is a scaled (slow) time. Note that the long-wave approximation leads to the neglect of the lateral diffusion term C_{xx}. This neglect is justified only far away from the stagnation point at $x = 0$ but makes tractable the solution of the linear-stability problem.

The nonparallel flow gives rise to the term xC_x that is scale invariant and so survives the long-wave approximation. The system can be solved by employing quasinormal modes as follows:

$$C(x,\zeta,\tau) = e^{\sigma\tau + ia\ln x}C(\zeta) \qquad [15]$$

These modes convert the system into a constant-coefficient eigenvalue problem for the growth rate $\sigma = \sigma(k, M; a)$. The system is solved numerically and Figures 7 and 8 show the neutral curves and the imaginary part of σ on the neutral curve.

The flow produces a long-wave instability that creates waves that travel inward, toward the stagnation point. It is locally periodic in x but, by the structure of the normal modes, is not globally so. The instability exists for long waves, in a region where the Mullins and Sekerka condition gives only stability. Thus, it is called flow-induced morphological instability. The largest growth rate (the real part of σ) occurs for a $a \to \infty$, where the long-wave theory is invalid and where surface energy should help stabilize the interface. Thus, "longish" waves would be preferred and these would grow for M just above unity, *i.e.*, for any degree of constitutional undercooling; thus, it is a morphological instability. The conjectured neutral stability curve, valid for all wave numbers, would be as shown in Figure 9. When the wave numbers are large, the disturbances see only the local velocities and the flow appears to be locally parallel. The dashed curve of Figure 9 shows the analog of the results of Coriell *et al.*[31] appropriate to locally parallel flows. When the wave numbers are small, the disturbances see the curvature of the streamlines and hence the nonparallel-flow effects found by Brattkus and Davis,[40] as shown in the solid curve of Figure 9. The connection between the small $|a|$ loop and the ordinary MI loop is conjectured.

The destabilization by nonparallel flow depends on both velocity components. The component normal to the mean position of the interface is directed inward. Its presence causes boundary-layer alteration. The concentration boundary layer is compressed, steepening the local gradient $|G_C|$. The lateral component of velocity (linear in x) varies with distance from the stagnation point and produces horizontal

concentration gradients that drive the traveling cells that propagate into the oncoming flow. Brattkus and Davis[40] argue that these instabilities may be responsible for the "rotational striations" present in crystals produced in devices using crystal rotation.

The destabilization of long waves in the x direction may be negated by "end" effects that disallow the "fitting" of such long waves in the system. In this case, the results of Coriell *et al.*[31] would be regained. One could then allow disturbances of the form

$$C(y,z,t) = e^{\sigma t + iby} C(z) \qquad [16]$$

for cross-stream periodic waves that are x independent ($a = 0$). The full stagnation-point flow linear-stability problem has been examined in this case by McFadden *et al.*[12] They find that the flow would then slightly delay morphological instability.

Merchant and Davis[43] considered temporally modulated stagnation-point flow. Here, the strength K of the stagnation-point flow is replaced by a time-periodic function as follows:

$$K \rightarrow K\Theta(\omega t) = K[1 + \delta \cos(\omega t)] \qquad [17]$$

They again considered long-wave two-dimensional disturbances and found that system (14) is replaced by the following:

$$C_{\zeta\zeta} + \left(1 + \frac{1}{2}\beta\Theta^{3/2}(\tau)\zeta^2\right)C_\zeta - \beta\Theta^{3/2}(\tau)x\zeta C_x = \gamma C_\tau,\ 0 \le \zeta < \infty \qquad [18a]$$

$$C_\zeta + \gamma(1 - M^{-1})C_\tau + [k(1 - M^{-1})^{-1} + (1 - k)]C = 0,\ \zeta = 0 \qquad [18b]$$

$$C = 0,\ \zeta \rightarrow \infty \qquad [18c]$$

where $\gamma = \omega D/V^2$ is the scaled forcing frequency. They found that modulation at low frequency stabilizes the interface against flow-induced morphological instabilities while high frequency promotes the instabilities. The response of the system to instability is quite complex, with a disturbance being composed of two independent frequencies, the imposed frequency and the traveling-wave frequency modified by the modulation.

C. *Unsteady Parallel Flows*

While the studies described so far have added insight into the interplay between forced flows and morphological instability, they have not added significantly to one's ability to control interfacial morphology. The flows described so far have one or more of the following shortcomings when it comes to stabilizing the interface: (1) stabilization is achieved only for a restricted range of wavenumbers and there is subsequent introduction of new longwave, flow-induced instabilities; (2) stabilization is found in only two dimensions, with only pattern-selection capability in three dimensions; and (3) the stabilization is only of small magnitude. In this section, we describe the work of Schulze and Davis[44,45] on directional solidification into Stokes boundary layers and related flows. It turns out that each of these concerns can be alleviated by choosing an appropriate oscillatory flow parallel to the interface.

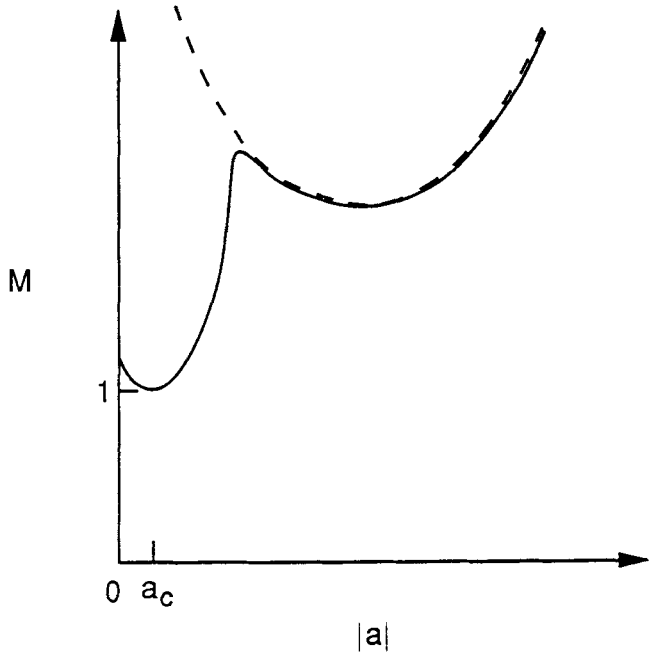

Fig. 9—Directional solidification into stagnation-point flow: Conjectured neutral curve, M *vs* $|a|$, shown as the solid curve for general two-dimensional disturbances on a Hiemenz flow against a solidifying interface according to Brattkus and Davis.[40,41] For small a, nonparallel effects dominate; for other a, the curve coincides with the locally parallel theory of Coriell *et al.*,[31] as shown by the dashed curve.

We begin by considering the directional solidification into a Stokes boundary layer. This flow can be generated by zero-mean unidirectional oscillations of the crystal back and forth, parallel to the interface, during the solidification process. The Stokes boundary layer will be compressed due to the flow normal to the interface generated by the pulling velocity. We refer to this flow configuration as the compressed Stokes layer (CSL).

The equations governing the system in the fluid region are the Navier–Stokes, continuity, and solute diffusion equations. To simplify the analysis, we once again make use of the frozen-temperature approximation. In nondimensional form, these equations are

$$\Omega\mathbf{u}_t + \varepsilon\mathbf{u}\cdot\nabla\mathbf{u} - \mathbf{u}_z = -\nabla p + S\nabla^2\mathbf{u} \qquad [19a]$$

$$\nabla\cdot\mathbf{u} = 0 \qquad [19b]$$

$$\Omega C_t + \varepsilon\mathbf{u}\cdot\nabla C - C_z = \nabla^2 C \qquad [19c]$$

$$T = z \qquad [19d]$$

We have nondimensionalized the equations using the following scalings:

$$\mathbf{x} \rightarrow (D/V)\mathbf{x},\ \mathbf{u} \rightarrow \mathbf{U}\mathbf{u},\ t \rightarrow t/\omega \qquad [20a]$$

$$p \rightarrow \rho UVp,\ T \rightarrow (GD/V)T + T_0,\ C \rightarrow (C_\infty - C_\infty/k)C + C_\infty/k \qquad [20b]$$

where D is the solute diffusivity, V is the crystal pulling speed, U is the amplitude of the velocity oscillations, ρ is the material density, C_∞ is the far-field concentration, ω is the angular frequency of the elliptical oscillations of the crystal, G is the thermal gradient, T_0 is the temperature of the interface in the basic state, and k is the segregation coefficient.

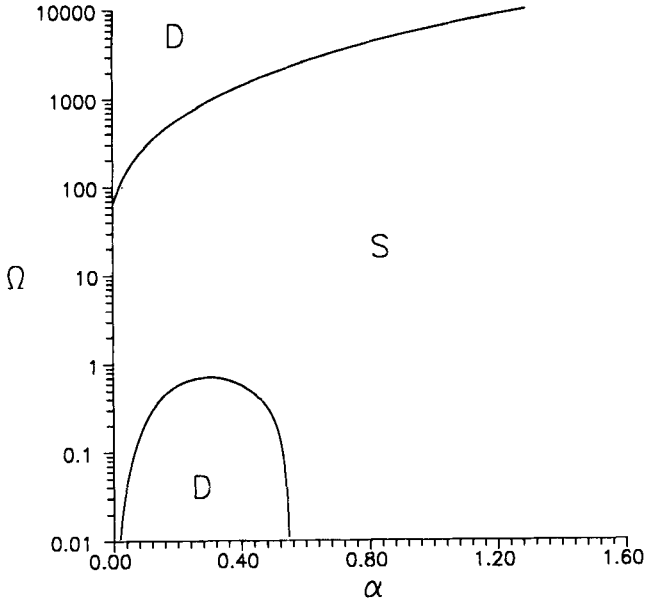

Fig. 10—Directional solidification into CSL: Regions of the α-Ω plane where the flow stabilizes (S) or destabilizes (D) the interface relative to the case without flow. $S = 81.0$, $k = 0.3$, and $\varepsilon << 1$, according to Schulze and Davis,[44,45] results are independent of Γ.

The nondimensional parameters that appear in the equations and boundary conditions are the morphological number M, the surface energy parameter Γ, the Schmidt number S, the nondimensional angular frequency Ω, the segregation coefficient k, and a parameter ε measuring the amplitude of the lateral oscillations in units of pulling speed:

$$M = \frac{mVC_\infty(1 - 1/k)}{GD}, \Gamma = \frac{T_m\gamma V}{DL_v mC_\infty(1 - 1/k)} \quad [21a]$$

$$S = \frac{\nu}{D}, \Omega = \frac{\omega D}{V^2}, \varepsilon = \frac{U}{V} \quad [21b]$$

The interfacial conditions, evaluated at the interface $z = h(x, y, t)$, are mass balance and no slip, a nondimensional version of the Gibbs–Thomson equation, and a balance of solute flux across the interface. We also assume appropriate far-field conditions.

The basic state for this system takes the form

$$\overline{u} = e^{-Bz}\cos(t - Az) \quad [22a]$$

$$\overline{v} = \overline{w} = \overline{h} = 0 \quad [22b]$$

$$\overline{C} = 1 - e^{-z} \quad [22c]$$

where A and B are known constants whose values depend on S and Ω.

To analyze the response of this state to infinitesimal perturbations, one disturbs each of these quantities and separates the disturbances into normal modes of the form

$$\phi = \overline{\phi} + \hat{\phi}(z,t)e^{i(\alpha_1 x + \alpha_2 y)}e^{\sigma t} + cc \quad [23]$$

where $\alpha = \sqrt{\alpha_1^2 + \alpha_2^2}$ is the overall wavenumber. Here, we are seeking time-periodic eigenfunctions with the same period as the basic state, and σ is the Floquet exponent. If the real part of σ is not zero, then the disturbances will experience a net growth or decay over one period.

Routine algebraic manipulations result in two linearized disturbance equations for the solute concentration and vertical component of the velocity.

Figure 10 maps out the regions of the α-Ω plane where the flow has a stabilizing influence on the interface for a small-amplitude flow $\varepsilon << 1$. Notice that there is a range of frequencies for which all finite wavenumbers are stabilized. This is a *window of stabilization.*

It turns out that the CSL, like the parallel flows mentioned previously, is only able to stabilize in two dimensions. In three dimensions, only disturbances with wavevectors aligned with the parallel flow will be stabilized, while those with wavevectors perpendicular to the flow are unaffected; thus, the flow acts as a pattern selection mechanism only. Note, however, that the stabilization can be achieved for all wavenumbers, eliminating the potential introduction of new flow-induced morphological instabilities.

Motivated by the work of Kelly and Hu[46] on Bénard convection, Schulze and Davis[45] extend the stabilizing influence of the CSL to three dimensions by considering the influence of nonplanar oscillations. Specifically, they consider the effect of adding a second oscillation perpendicular to the first which has the same frequency but may differ in amplitude and phase. The boundary conditions at the interface then read

$$u = \cos t \quad [24a]$$

$$v = \lambda\cos(t + \gamma) \quad [24b]$$

where λ is the ratio of the amplitudes of the two oscillations and γ is the phase difference between them. This corresponds to translating the crystal in elliptical orbits parallel to the interface. Circular orbits are optimal for stabilization purposes, and all of the results reported here are for that case.

It turns out that if the two oscillations are either perfectly in or out of phase, the resulting flow is equivalent to a Stokes layer. This means that within the window of stabilization found previously, the flow acts only as a pattern selection mechanism, with cells oriented along the flow direction.

When the phase between the oscillations is not a multiple of π, it is possible to stabilize an arbitrary three-dimensional disturbance within the window of stabilization found previously. Thus, the ability of the nonplanar oscillations to stabilize the interface is predicted by the results for the CSL, and the window of stabilization is the same for both cases. The stability results that we have discussed to this point are for a weak flow, and subsequently, only a small amount of stabilization is achieved.

Having shown that a small amount of stabilization can be achieved in three dimensions for arbitrary disturbances, Schulze and Davis[45] demonstrate that the interface can be completely stabilized in many instances by increasing the strength of the flow and, hence, the value of ε. Following the method used by Hall[47] for the Stokes layer, they find an exact solution for the system in the form of an infinite Fourier series in time. They then truncate this series to produce numerical results.

Guided by the results for weak oscillations, they choose the value $\Omega = 10$ for the nondimensional forcing frequency. This lies within the window of stabilization found previously and is close to the optimal frequency for stabi-

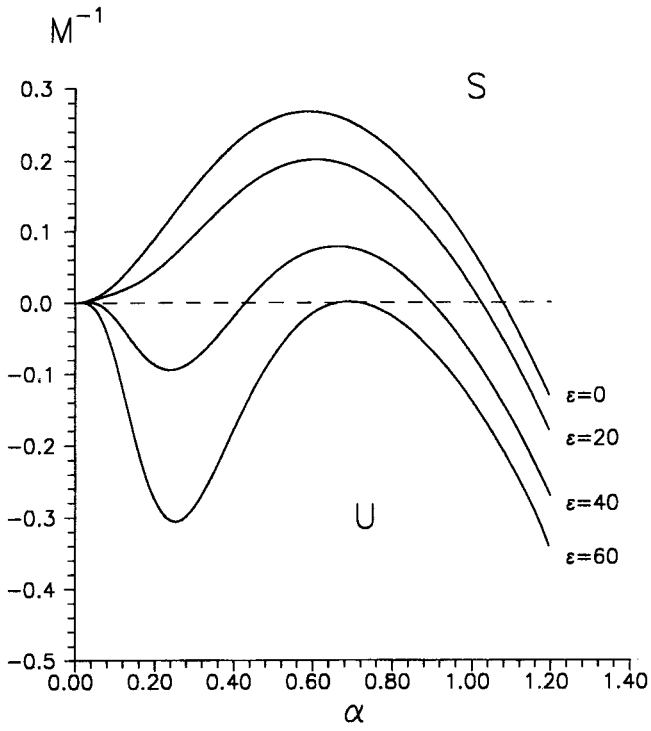

Fig. 11—Directional solidification into CSL: Plot of M^{-1} as a function of α for $k = 0.3$, $S = 81.0$, $\Gamma = 0.6$, $\Omega = 10.0$, and $\varepsilon = \{0, 20, 40, 60\}$, according to Schulze and Davis.[45] The region above each curve corresponds to a linearly stable (S) interface, and the region below each curve corresponds to a linearly unstable (U) interface. As ε increases, the critical value of M^{-1} decreases. Notice that for $\varepsilon \approx 60$, the interface is absolutely stable.

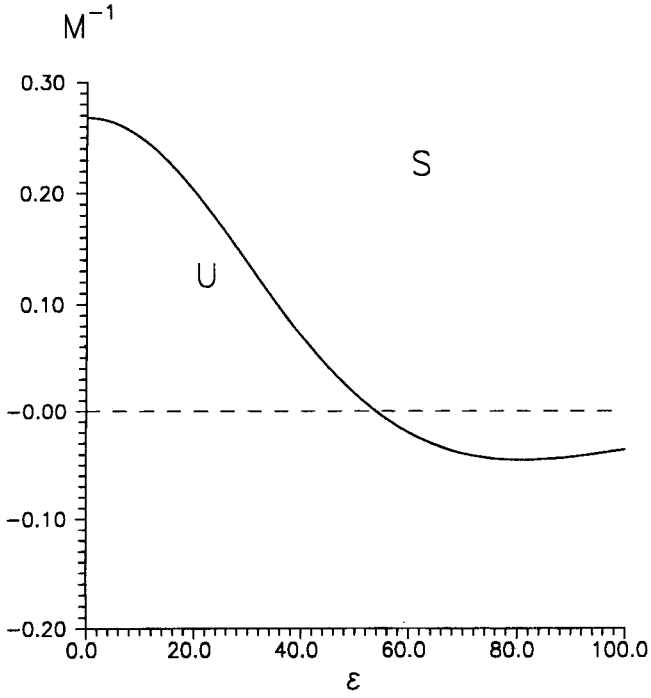

Fig. 12—Directional solidification into CSL: Plot of M^{-1} *vs* ε with $\alpha = \alpha_c$ (the critical value for the no-flow case), according to Schulze and Davis.[45] $k = 0.3$, $S = 81.0$, and $\Omega = 10.0$. This plot shows that the stabilizing trend eventually reverses as ε is increased.

lization purposes. Figure 11 is a plot of M^{-1} *vs* α for speed ratios $\varepsilon = \{0, 20, 40, 60\}$. Recall that when $\varepsilon = 0$, we

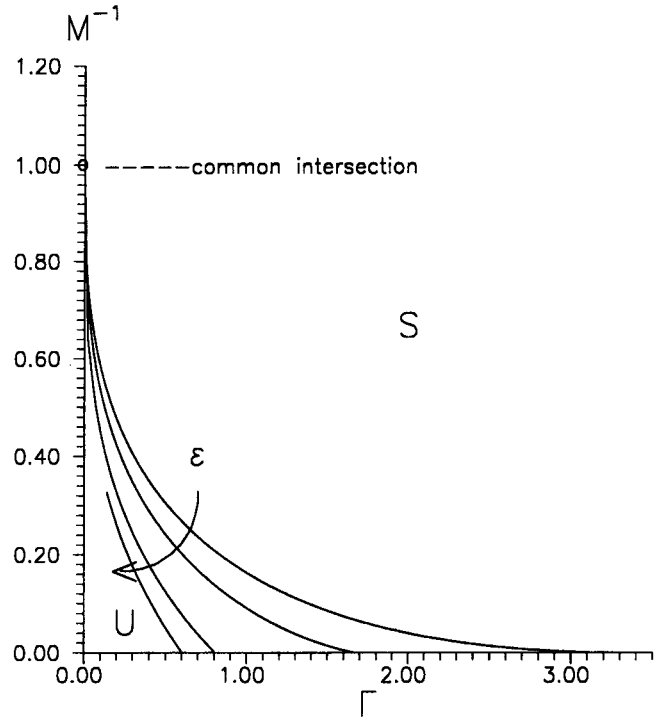

Fig. 13—Directional solidification into CSL: Plot of the critical value of M^{-1} as a function of Γ for $k = 0.3$, $S = 81.0$, $\Omega = 10.0$, and $\varepsilon = \{0, 20, 40, 60\}$, according to Schulze and Davis.[45] The arrow indicates the direction in which ε increases. The interface is linearly stable (S) when the inverse morphological number is above the neutral curve. All of the curves terminate at the point ($\Gamma = 0$, $M^{-1} = 1$). Notice that the range of parameter values for which the interface is stable increases with ε.

recover the no-flow results of Mullins and Sekerka, as shown in Figure 2. Notice that for $\varepsilon = 60$, the neutral curve lies entirely beneath the horizontal axis, indicating that the instability has been eliminated for all physically realizable morphological numbers. Also notice that as the neutral curve drops below the horizontal axis, there is an abrupt shift in the critical wavenumber from a finite value to zero.

These calculations were done for the two-dimensional case (CSL). Schulze and Davis verified that the instability may be entirely suppressed in three dimensions by using an amplitude ratio $\lambda = 1$ and a phase difference of $\pi/2$. In this case, the suppression of disturbances is independent of their orientation θ, and the dependence on wavenumber is identical to that of the two-dimensional case.

If one continues to increase ε past the value necessary to stabilize the interface, one finds, for these material parameters and operating conditions, that the stabilization trend is reversed. This is demonstrated in Figure 12, which is a plot of M^{-1} *vs* ε with $\alpha = \alpha_c$, the critical value in the absence of flow. This may indicate that there is an amplitude window as well as a frequency window for stabilization. Calculations for larger values of ε were not made due to the increasing difficulty of performing these computations, which results from the large number of modes needed for convergence.

Figure 13 is a plot of the critical value of M^{-1} as a function of Γ for $\varepsilon = \{0, 20, 40\}$. When $\varepsilon > 0$, this result depends on the segregation coefficient, Schmidt number, and forcing frequency. This figure again uses the values $k = 0.3$, $S = 81.0$, and $\Omega = 10.0$. As mentioned earlier, the nondimensional critical wavenumber approaches infinity as

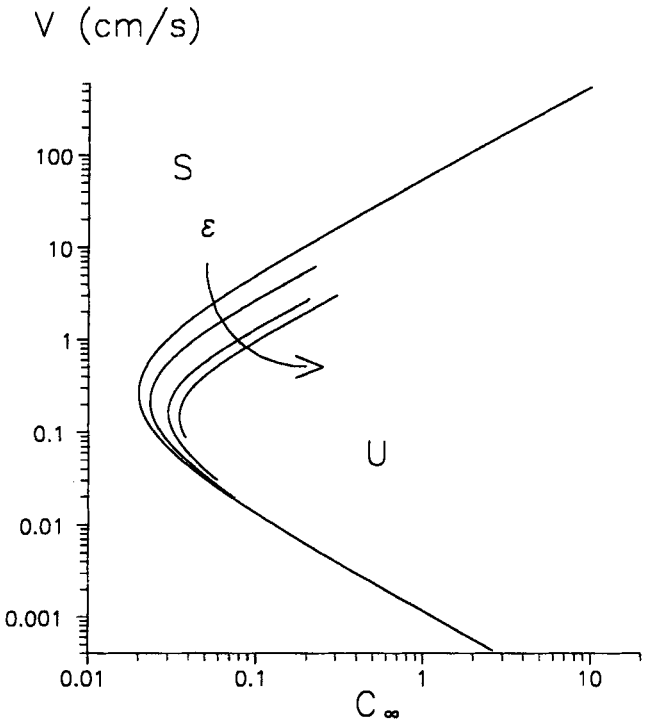

Fig. 14—Directional solidification into CSL: Plot of the neutral curve in dimensional form—V *vs* C_∞ for $k = 0.3$, $S = 81.0$, $\Omega = 10.0$, and $\varepsilon = \{0, 20, 40, 60\}$, according to Schulze and Davis.[45] The arrow indicates the direction in which ε increases. The temperature gradient G is 200 K/cm. All of the curves extend infinitely along tangents to the portions shown. The interface is linearly stable (S) when the far-field concentration is to the left of the neutral curve. Notice that the stability of the interface increases with ε.

$\Gamma \to 0$ along these curves and, for small values of ε, approaches zero as Γ is increased. Notice that the flow has a diminishing effect on stability as Γ approaches zero and that the neutral curve always passes through $M^{-1} = 1$ when $\Gamma = 0$. As ε is increased, the absolute stability limit Γ_s decreases, and for larger values of ε, the critical wavenumber no longer approaches zero as Γ approaches the absolute stability limit.

In Figure 14, we reproduce the information from Figure 13 in terms of dimensional variables, plotting the pulling speed V as a function of the far-field concentration C_∞ with the temperature gradient G fixed at 200 K/cm. From this figure, we see that if the far-field concentration C_∞ is sufficiently large, the interface will be unstable for a range of pulling speeds. The critical wavenumber, in units of D/V, approaches infinity along the lower branch of this curve and zero along the top branch. The stable regime lies to the left of the curve. We have previously noted that as ε is increased, the interface becomes more stable. This result is evident in Figure 14; for as ε is increased, the nose of the neutral curve is shifted downward and to the right, and the upper branch of the curve is lowered. The lower branch of this curve is relatively unaffected, however.

In general, the interface becomes increasingly difficult to stabilize as the surface energy parameter Γ is reduced. The necessary values of ε and Ω needed to achieve stabilization for all morphological numbers for small Γ may not be obtainable in practice. Formulas for determining the dimensional radius r and angular frequency ω of the circular motion in terms of the nondimensional quantities and the pulling speed V are

$$r = U/\omega = \varepsilon D/V\Omega \qquad [25a]$$

$$\omega = V^2\Omega/D \qquad [25b]$$

Murray *et al.*[48,49] and Wheeler *et al.*[50] have looked at the effect of gravity modulation (g-jitter) on the onset of solutal convection during directional solidification. While these articles do not address morphological instability, they are closely related to the articles discussed in this section.

V. SUMMARY

In this article, we have discussed the directional solidification of binary alloys. We have seen that morphological instability can be promoted or retarded by flow and that new instabilities, generating complex morphologies, can be created by flow in situations where the Mullins and Sekerka criterion predicts that planar fronts are stable.

In the case of steady, parallel shear flows, we saw that disturbances periodic in the direction of the flow are stabilized if they have a short wavelength but are destabilized if they have a long wavelength. Thus, if the instability in the absence of flow is characterized by a long wavelength, the flow will destabilize the interface. These long-wave instabilities are not seen unless one properly accounts for the boundary layer structure of the flow. If the instability in the absence of flow has a short wavelength, then disturbances in the flow direction will be stabilized; however, the cross-stream disturbances will be unaffected. Thus, the flow acts as a pattern selection mechanism in this case.

Flow-induced, longwave, morphological instabilities were also seen in the presence of a stagnation-point flow. Low-frequency modulation of the stagnation-point flow was seen to stabilize the interface against this instability, while high-frequency modulation was seen to promote the instability.

When an unsteady, parallel shear flow is generated by oscillating the crystal back and forth, one finds that disturbances periodic in the flow direction are stabilized for both long and short wavelength disturbances. As with the steady shear flows, however, disturbances in the cross-stream direction are unaffected.

One can extend the stabilizing influence of the unsteady shear flow to three dimensions by adding a second oscillation of the crystal perpendicular to, and out of phase with, the first. This corresponds to translating the crystal in elliptical orbits parallel to the interface. In this case, one finds that the critical morphological number for the Mullins and Sekerka instability is always higher than in the case without flow. If surface energy is not too weak, one may eliminate the instability, on a linear theory basis, for all morphological numbers by using oscillations with sufficiently large forcing amplitude.

REFERENCES

1. F. Rosenberger: *Fundamentals of Crystal Growth I*, Springer, New York, NY, 1979.
2. R.A. Brown: *AIChE J.*, 1988, vol. 34, p. 881.
3. M.E. Glicksman, S.R. Coriell, and G.B. McFadden: *Ann. Rev. Fluid Mech.*, 1986, vol. 18, p. 307.
4. S.H. Davis: *J. Fluid Mech.*, 1990, vol. 212, p. 241.

5. S.H. Davis: in *Handbook of Crystal Growth*, D.T.J. Hurle, ed., North-Holland Press, Amsterdam, 1993, p. 859.
6. J.R. Carruthers: in *Treatise on Solid State Chemistry*, N.B. Hannay, ed., Plenum Press, New York, NY, 1975, vol. 5, p. 323.
7. J.R. Carruthers: in *Preparation and Properties of Solid State Material*, W.R. Wilcox and R.A. Lefever, eds., Marcel Dekker, New York, NY, 1977, p. 1.
8. J.R. Carruthers: in *Crystal Growth: A Tutorial Approach*, W. Bardsley, D.T.J. Hurle, and J.B. Mullin, eds., North-Holland Press, Amsterdam, 1979, p. 157.
9. D.T.J. Hurle: in *Crystal Growth and Materials*, E. Kaldis and H.J. Scheel, eds., North-Holland Press, Amsterdam, 1977, p. 550.
10. A. Solan and S. Ostrach: in *Preparation and Properties of Solid State Materials*, W.R. Wilcox, ed., Marcel Dekker, Amsterdam, 1979, vol. 4, p. 63.
11. S.M. Pimputkar and S. Ostrach: *J. Cryst. Growth*, 1981, vol. 55, p. 614.
12. N. Kobayashi: in *Preparation and Properties of Solid State Materials*, W.R. Wilcox, ed., Marcel Dekker, Amsterdam, 1981, vol. 6, p. 119.
13. M.A. Azouni: *Physicochem. Hydrodyn.*, 1981, vol. 2, p. 295.
14. F. Rosenberger: in *Convective Transport and Instability Phenomena*, J. Zeirep and H. Oertl, Jr., eds., G. Braun, Karlsruhe, 1982, p. 469.
15. S. Ostrach: *J. Fluids Eng.*, 1983, vol. 105, p. 5.
16. W.E. Langlois: *Physicochem. Hydrodyn.*, 1981, vol. 2, p. 245.
17. W.E. Langlois: *Ann. Rev. Fluid Mech.*, 1985, vol. 17, p. 191.
18. S.R. Coriell, G.B. McFadden, and R.F. Sekerka: *Ann. Rev. Mater. Sci.*, 1985, vol. 15, p. 119.
19. W.W. Mullins and R.F. Sekerka: *J. Appl. Phys.*, 1964, vol. 35, p. 444.
20. J.W. Rutter and B. Chalmers: *Can. J. Phys.*, 1953, vol. 31, p. 15.
21. J.W. Boettinger, D. Shechtman, R.J. Schaefer, and F.S. Biancaniello: *Metall. Trans. A*, 1984, vol. 15A, pp. 55-66.
22. R. Trivedi, J.A. Sekhar, and J.A.V. Seetharaman: *Metall. Trans. A*, 1989, vol. 20A, pp. 769-77.
23. J.S. Langer: *Rev. Mod. Phys.*, 1980, vol. 52, p. 1.
24. W.A. Tiller, K.A. Jackson, J.W. Rutter, and B. Chalmers: *Acta Metall.*, 1953, vol. 1, p. 428.
25. D.J. Wollkind and L.A. Segel: *Phil. Trans. R. Soc. London A*, 1970, vol. 268, p. 351.
26. B. Caroli, C. Caroli, and B. Roulet: *J. Phys. (Paris)*, 1982, vol. 43, p. 1767.
27. J.I.D. Alexander, D.J. Wollkind, and R.F. Sekerka: *J. Cryst. Growth*, 1986, vol. 79, p. 849.
28. S.R. Coriell and G.B. McFadden: in *Handbook of Crystal Growth*, D.T.J. Hurle, ed., North-Holland Press, Amsterdam, 1993, p. 785.
29. R.T. Delves: *J. Cryst. Growth*, 1968, vols. 3–4, p. 562.
30. R.T. Delves: *J. Cryst. Growth*, 1979, vol. 8, p. 13.
31. S.R. Coriell, G.B. McFadden, R.F. Boisvert, and R.F. Sekerka: *J. Cryst. Growth*, 1984, vol. 69, p. 514.
32. S.A. Forth and A.A. Wheeler: *J. Fluid Mech.*, 1989, p. 202.
33. S.A. Forth and A.A. Wheeler: *J. Fluid Mech.*, 1992, vol. 236, p. 61.
34. A.K. Hobbs and P. Metzener: *J. Cryst. Growth*, 1991, vol. 112, p. 539.
35. A.K. Hobbs and P. Metzener: *J. Cryst. Growth*, 1992, vol. 118, p. 319.
36. K. Brattkus and S.H. Davis: *Phys. Rev.*, 1988, vol. B38, p. 11452.
37. L.A. Segel: *J. Fluid Mech.*, 1969, vol. 38, p. 203.
38. A.C. Newell and J.A. Whitehead: *J. Fluid Mech.*, 1969, vol. 38, p. 279.
39. Y. Kuromoto: *Chemical Oscillations, Waves, and Turbulence*, Springer-Verlag, Berlin, 1984.
40. K. Brattkus and S.H. Davis: *J. Cryst. Growth*, 1988, vol. 87, p. 385.
41. K. Brattkus and S.H. Davis: *J. Cryst. Growth*, 1988, vol. 89, p. 423.
42. G.B. McFadden, S.R. Coriell, and J.I.D. Alexander: *Comm. Pure Appl. Math.*, 1988, vol. 41, 683.
43. G.J. Merchant and S.H. Davis: *J. Cryst. Growth*, 1989, vol. 96, p. 737.
44. T.P. Schulze and S.H. Davis: *J. Cryst. Growth*, 1994, vol. 143, p. 317.
45. T.P. Schulze and S.H. Davis: *J. Cryst. Growth*, 1995, vol. 49, p. 253.
46. R.E. Kelly and H.-C. Hu: *J. Fluid Mech.*, 1993, vol. 249, p. 373.
47. P. Hall: *Proc. R. Soc. London A*, 1978, vol. 359, p. 151.
48. B.T. Murray, S.R. Coriell, and G.B. McFadden: *J. Cryst. Growth*, 1991, vol. 110, p. 713.
49. B.T. Murray, S.R. Coriell, G.B. McFadden, A.A. Wheeler, and B.V. Saunders: *J. Cryst. Growth*, 1993, vol. 129, p. 70.
50. A.A. Wheeler, G.B. McFadden, B.T. Murray, and S.R. Coriell: *Phys. Fluids A*, 1991, vol. 3, p. 2847.